Therapeutic Targeting of Neuropilin-2 on Colorectal Carcinoma Cells Implanted in the Murine Liver

Michael J. Gray, George Van Buren, Nikolaos A. Dallas, Ling Xia, Xuemei Wang, Anthony D. Yang, Ray J. Somcio, Yvonne G. Lin, Sherry Lim, Fan Fan, Lingegowda S. Mangala, Thiruvengadam Arumugam, Craig D. Logsdon, Gabriel Lopez-Berestein, Anil K. Sood, Lee M. Ellis

Background Neuropilin-2 (NRP2) is a high-affinity kinase-deficient receptor for vascular endothelial growth factor (VEGF) and semaphorin 3F. We investigated its function in human colorectal cancers.

Methods Immunohistochemistry and immunoblotting were used to assess NRP2 expression levels in colorectal tumors and colorectal cancer cell lines, respectively. HCT-116 colorectal cancer cells stably transfected with short hairpin RNA (shRNAs) against NRP2 or control shRNAs were assayed for proliferation by the tetrazolium salt 3-(4,5-dimethylthiazol-2-yl)-2,5-diphenyltetrazolium bromide (MTT) assay and for activation of the VEGFR1 pathway by immunoblotting. Soft agar assays, Annexin V staining, and Boyden chamber assays were used to examine anchorage-independent growth, apoptosis in response to hypoxia, and cell migration/invasion, respectively, in HCT-116 transfectants. Tumor growth and metastasis were analyzed in mice (groups of 10) injected with shRNA-expressing HCT-116 cells. The effect of in vivo targeting of NRP2 by small interfering RNA (siRNA) on the growth of hepatic colorectal tumors derived from luciferase-expressing HCT-116 cells was assessed by measuring changes in bioluminescence and final tumor volumes. All statistical tests were two-sided.

Results NRP2 expression was substantially higher in tumors than in adjacent mucosa. HCT-116 transfectants with reduced NRP2 levels had reduced VEGFR1 signaling, but proliferation was unchanged. Anchorage-independent growth, survival under hypoxic conditions, and motility/invasiveness were also reduced. In vivo, HCT-116 transfectants with reduced NRP2 demonstrated decreased tumor growth, fewer metastases, and increased apoptosis compared with control cells. Hepatic colorectal tumors in mice treated with NRP2 siRNAs were statistically significantly smaller than those in mice treated with control siRNAs (at 28 days after implantation, mean control siRNAs = 420 mm^3, mean NRP2 siRNAs = 36 mm^3, NRP2 vs control: difference = 385 mm^3, 95% confidence interval = 174 mm^3 to 595 mm^3, $P = .005$).

Conclusion NRP2 on colorectal carcinoma cells is important for tumor growth and is a potential therapeutic target in human cancers where it is expressed.

J Natl Cancer Inst 2008;100:109–120

Tumor angiogenesis is a complex process that requires interactions among endothelial cells, tumor cells, and other components of the microenvironment. Among numerous secreted factors that promote angiogenesis, perhaps the most important is vascular endothelial growth factor (VEGF) (1,2). VEGF-A is the most prominent and biologically active member of the VEGF family, which also includes VEGF-B, VEGF-C, VEGF-D, VEGF-E, and placental growth factor (2,3). The activity of the VEGF family is mediated by the VEGF tyrosine kinase receptors VEGFR1, VEGFR2, and VEGFR3 (4). Initially, these receptors were believed to be expressed only on the surface of endothelial cells, but subsequent findings have revealed that VEGF tyrosine kinase receptors are expressed on numerous human cancer cells as well [reviewed in (5)].

Two additional VEGF receptors, neuropilin-1 (NRP1) and neuropilin-2 (NRP2), have also been recently implicated in VEGF-mediated vascularization and lymphangiogenesis (6–8). NRP1 and NRP2 were originally identified as neuronal patterning receptors for the class 3 semaphorin ligands (Sema3A, Sema3C, and Sema3F) (9,10). Unlike the previously identified VEGF receptors, NRP1 and NRP2 lack a tyrosine kinase domain. Although the precise mechanisms for their activities are still a

Affiliations of authors: Departments of Cancer Biology (LX, RJS, FF, TA, CDL, AKS, LME), Gynecologic Oncology (YGL, LSM, AKS), Experimental Therapeutics (GLB), Qualitative Sciences (XW), and Surgical Oncology (MJG, GVB, NAD, ADY, SL, LME), The University of Texas M. D. Anderson Cancer Center, Houston, TX.

Correspondence to: Lee M. Ellis, MD, Department of Surgical Oncology, Unit 444, The University of Texas M. D. Anderson Cancer Center, PO Box 301402, Houston, TX 77230-1402 (e-mail: lellis@mdanderson.org).

See "Funding" and "Notes" following "References."

DOI: 10.1093/jnci/djm279

CONTEXT AND CAVEATS

Prior knowledge

The neuropilins, a class of nonkinase cell surface receptors that bind VEGF and class III semaphorins, appear to enhance the activity of VEGF tyrosine kinase receptors in response to VEGF. The neuropilins are not normally expressed in nonvascular adult tissues but neuropilin-1 is present on some tumor cells, and inhibitors of neuropilin-1 have been shown to be effective in reducing tumor growth.

Study design

Expression of neuropilin-2 (NRP2) was examined in colorectal tumors and cell lines. HCT-116 colorectal cancer cells stably transfected with short hairpin RNAs to NRP2 were used to assess the role of NRP2 in cell proliferation, anchorage-independent growth, apoptosis, migration, invasion, and tumorigenesis. Liposomes carrying small interfering RNAs (siRNAs) to NRP2 were used to treat hepatic tumors derived from HCT-116 cells implanted in mice.

Contribution

NRP2 was expressed on tumors but not normal tissue. Blocking NRP2 function reduced anchorage-independent growth, cell survival under hypoxic conditions, cell migration, invasiveness, and tumorigenicity. Finally, therapeutic targeting of NRP2 was validated by its efficacy in treating tumor xenografts in mice.

Implications

NRP2 appears to be a promising target, possibly in combination with anti-VEGF therapies, for the treatment of human cancers.

Limitations

Only HCT-116 human colorectal carcinoma cells were used for most functional assays in the study. Whether the siRNAs used inhibit VEGF-dependent or -independent activities of NRP2 remains unclear.

matter of debate, most studies suggest that the NRPs function as obligate coreceptors by cooperatively enhancing the activity of the VEGF kinase receptors in nonneuronal tissues (6,11–15). Although NRP1 and NRP2 are not normally expressed in adult tissues, their expression is detected on some human tumor cells (6,7). Preliminary reports suggest that carcinomas primarily express NRP1, whereas neural tumors and melanomas largely express NRP2 [reviewed in (7)]. NRP1 function has been studied in numerous tumor types, sometimes with conflicting results, but the expression and function of NRP2 on tumor cells has yet to be elucidated (6,7).

To date, most anti-VEGF therapeutic targeting has focused on attenuation of VEGFR2 kinase activity. Although anti-VEGF–targeted therapies for patients with cancer have led to incremental improvements in efficacy, the overall outcomes (eg, prolonged tumor dormancy) have not met expectations (16,17). The relatively disappointing performance of anti-VEGF system therapies in the clinic suggests that further refinements are required for these agents to produce greater benefits in terms of long-term patient survival. Alternative anti-VEGF therapies may include direct targeting of the NRPs: for example, interruption of NRP1 function with a monoclonal antibody in tumor-associated endothelial cells has been shown to have additive effects when used in conjunction with anti-VEGF therapy (15,16).

The expression and function of the VEGF receptors, in particular NRP2, in colorectal carcinoma cells remain largely unknown. In this study, we examined NRP2 expression in colorectal tumors, adjacent uninvolved mucosa, and in colorectal cancer cells. Additionally, we constructed stable colorectal cancer cell lines that expressed NRP2-directed or control short hairpin RNAs (shRNAs) to assess the effect of reducing NRP2 expression on VEGFR1 signaling, cell proliferation, anchorage-independent growth, susceptibility to apoptosis, cell migration, invasion, and tumorigenicity in nude mice. Finally, through the use of bioluminescence imaging of genetically engineered colon cancer cells, we examined the validity of therapeutic targeting of human NRP2 with small interfering RNAs (siRNAs) on colorectal carcinoma cells implanted in the murine liver.

Materials and Methods

Tissue Specimens and Cell Lines

Specimens of colon adenocarcinoma, adjacent nonmalignant colonic mucosa, and colon cancer liver metastases were obtained from an established tissue bank in the Department of Surgical Oncology at The University of Texas M. D. Anderson Cancer Center (MDACC), following protocols approved by the institutional review board of MDACC. Specimens were fixed in formalin at the time of collection. Histopathologic confirmation was provided by the Department of Pathology at the MDACC.

The human colorectal carcinoma cell lines Geo, HCT-116, HT-29, RKO, and SW480 were obtained from the American Type Culture Collection (Manassas, VA). The human colorectal carcinoma cell line KM12 and the murine melanoma B16BL6 cell lines were obtained from Dr I. J. Fidler (MDACC). Unless stated otherwise, all cells were maintained at 37°C with 5% CO_2 in complete minimal essential medium supplemented with 10% fetal bovine serum, 2 mM L-glutamine, and 200 μg/mL streptomycin (Life Technologies, Grand Island, NY). For hypoxic studies, cells were plated at 80% density and were incubated at 37°C, 1% O_2, in an MCO-5M hypoxic chamber (Sanyo Scientific, Bensenville, IL). For VEGF-A stimulation studies, cells were incubated in minimal essential medium supplemented with 1% fetal bovine serum, 2 mM L-glutamine, and 200 μg/mL streptomycin. VEGF-A (R&D Systems, Minneapolis, MN) was used at a concentration of 10 μg/mL for 10 minutes.

shRNA Expression Plasmids, shRNA Cell Lines, and Transient siRNA Targeting

shRNA expression vectors were created with the use of pSilencer 4.0 shRNA expression system (Ambion, Austin, TX) following the manufacturer's directions. Using the Ambion siRNA web design tool (www.Ambion.com), we identified two potential NRP2-specific target sequences (NP2-#1: 5′-AAGCTCTGGGCATGGAATCAG-3′ and NP2-#2: 5′-AAAGCCCCGGGTACCTTACAT-3′). Two annealed oligonucleotides, each encoding one of the target sequences followed by a 9-bp hairpin sequence (TTCAAGAGA) and flanked by 5′ *Bam*HI and 3′ *Hin*dIII overhangs, were ligated into the pSilencer 4.0 expression plasmid at compatible sites. The two resulting shRNA expression plasmids, sh-NP2Vec-#1 and sh-NP2Vec-#2, were confirmed by sequencing. For negative controls,

shRNA vectors were created using a scrambled sequence of each of the NRP2 target sequences (Con-#1, 5′-AGATCGGTGGCCTA TAGAACG-3′ and Con-#2, 5′-GATCATCACCTTGGACCA GAC-3′). Sequences were confirmed by NIH BLAST analysis to have no substantial homology to sequences in other vertebrate genes. Control shRNA control plasmids were designated sh-ConVec-#1 and sh-ConVec-#2. The NRP2 deficient cell lines sh-NP2-C8 and sh-NP2-C9 were each created by transfecting HCT-116 cells with 0.5 ng of both shRNA expression plasmids (sh-NP2Vec-#1 and sh-NP2Vec-#2), and control shRNA cells were created by transfecting HCT-116 cells with 0.5 ng of both scrambled sequence encoding shRNA vectors (sh-ConVec-#1 and sh-ConVec-#2). Stable clones were isolated by growing each transfected cell type in medium containing 850 μg/mL hygromycin B (Roche Diagnostics, Mannheim, Germany). NRP2 expression levels in isolated clones of shRNA-containing HCT-116 cells were determined by immunoblot analysis.

For transient transfections, 2.5×10^5 HCT-116 cells were plated per well in medium in 6-well plates and incubated for 24 hours. The cells were then transfected with increasing concentrations of siRNA oligonucleotides (both NP2-#1 and NP2-#2 without hairpins) using the transfection reagent SiPORT/NeoFX (Ambion) according to the manufacturer's protocol. The cells were incubated for an additional 72 hours after transfection and then solubilized in 100 μL of 20 mM Tris-HCl (pH 8.0), 137 mM NaCl, 1% Triton X-100, 1 mM Na_3VO_4, 2 mM EDTA, and one complete Mini Protease Inhibitor Cocktail Tablet (per 10 mL of lysis buffer) (Roche Diagnostics). Extracts were subjected to immunoblot analysis as described below to determine NRP2 levels.

Immunoprecipitation and Immunoblot Analyses

Immunoprecipitation and immunoblot analyses were performed as previously described (17), with minor modifications. Briefly, human colon carcinoma and murine melanoma cells were grown to 85%–90% confluence in 100-mm^3 plates in complete minimum essential medium (unless otherwise stated) and solubilized in 300 μL of 20 mM Tris-HCl (pH 8.0), 137 mM NaCl, 1% Triton X-100, 1 mM Na_3VO_4, 2 mM EDTA, and one complete Mini Protease Inhibitor Cocktail Tablet (per 10 mL of lysis buffer) (Roche Diagnostics). 50 μg of whole-cell lysates were separated by sodium dodecyl sulfate-polyacrylamide gel electrophoresis and transferred to polyvinylidene difluoride membranes (Amersham, Arlington Heights, IL) by electroblotting. All membranes were probed with antibodies at a concentration of 1 : 1000 unless otherwise stated. Antibodies used were as follows: NRP1 (C-19, Mu mAb, Santa Cruz Biotechnology, Santa Cruz, CA) and NRP2 (C-9 and/or H-300 from Santa Cruz Biotechnology); phospho-Akt^{Ser473} (DE-9, Rb mAb), Akt (C67E7, Rb mAb), phospho-$Erk\text{-}1/2^{Thr\ 202/Tyr204}$ (D13.14.4E, Rb mAb), Erk-1/2 (137F5, Rb mAb), phospho-BAD-Ser^{136} (9295 Rb mAb) and phospho-BAD-Ser^{112} (9291, Rb mAb), and BAD (9292, Rb pAb) (all from Cell Signaling Technology, Danvers, MA); phospho-$VEGFR1^{Tyr1213}$ (PC459, Rb pAb, Calbiochem, Boston, MA; 07-758, Rb pAb, Upstate/Millipore Corp., Billerica, MA); VEGFR1 (Oncogene Research Products, San Diego, CA). As a loading control, all membranes were stripped and reprobed for vinculin (V4505, Mu mAb, Sigma-Aldrich, St Louis, MO, 1 : 10 000 dilution). All antibodies were diluted in Tris-buffered saline and 0.1% (v/v) Tween-20 containing 5% dried milk. Membranes were incubated with the appropriate horseradish peroxidase–conjugated secondary antibodies, and antibody-bound proteins were visualized by chemiluminescence (New England Nuclear, Boston, MA).

Reverse Transcriptase-Polymerase Chain Reaction Assays

The relative expression levels of VEGFR1, VEGFR2, and VEGFR3 in human HCT-116 colon cancer cells and human umbilical vein endothelial cells (HUVEC) were determined by reverse transcriptase-polymerase chain reaction (RT-PCR) analysis. The primers used were VEGFR1, 5′-TGAAAGCCTTCAGTC CCGTG-3′ (sense), and 5′-ATCCGTGTTGAGGGTGGTCA GC-3′ (antisense); VEGFR2, 5′-CATCACATCCACTGGTATT GG-3′ (sense), and 5′-GCCAAGCTTGTACCATGTGAG-3′ (antisense); and VEGFR3, 5′-CCCACGCAGACATCAAGACG (sense), 5′-TGCAGAACTCCACGATCACC-3′ (antisense). RNA was extracted from HCT-116 cells and HUVECs using TRIzol reagent (Invitrogen, Carlsbad, CA) according to the manufacturer's protocol. For cDNA synthesis, 4 μg of total RNA of each sample was used with oligo-dT and Moloney Murine Leukemia Virus RT-polymerase (Epicenter, Madison, WI). Synthesized cDNAs were diluted in 500 μL of diethylpyrocarbonate-treated water, and 3 μL of each reaction was used in each 25-μL RT-PCR. DNA was amplified using the following parameters: 95°C for 1 minute, followed by 35 cycles of 95°C for 30 seconds, 60°C for 30 seconds and 72°C for 1 minute. VEGF receptor expression gene expression was normalized using reference primers for the glyceraldehyde 3-phosphate dehydrogenase (GAPDH) gene, 5′-CCTT CATTGACCTCAACTAC-3′ (sense), and 5′-GATGATGTTCT GGAGTGCC-3′ (antisense). PCR products were separated in a 1.2 % agarose gel and visualized by ethidium bromide staining.

Vascular Endothelial Growth Factor Enzyme-Linked Immunosorbent Assay

VEGF production in culture supernatants from control cells (parental HCT-116 cells and sh-Con transfectants) and HCT-116 cells with reduced NRP2 levels (sh-NP2-C8 and sh-NP2-C9 transfectants) was examined using a human VEGF-specific enzyme-linked immunosorbent assay (ELISA) according to the manufacturer's instructions (Quantikine; R&D Systems). Cells were plated at 80% cell density in a 100-mm cell culture dish in minimal essential medium supplemented with 1% fetal bovine serum, 2 mM L-glutamine, and 200 μg/mL streptomycin. After 24 hours, medium was removed for VEGF analysis, and cells were solubilized in 300 μL of 20 mM Tris-HCl (pH 8.0), 137 mM NaCl, 1% Triton X-100, 1 mM Na_3VO_4, 2 mM EDTA, and one complete Mini Protease Inhibitor Cocktail Tablet (per 10 mL of lysis buffer). VEGF concentration was normalized to the total protein content of each culture dish, as measured by the Bradford assay.

MTT Analysis of Cell Proliferation

Cell proliferation in vitro was analyzed with the tetrazolium salt 3-(4,5-dimethylthiazol-2-yl)-2,5-diphenyltetrazolium bromide (MTT) as described previously (18). The yellow dye MTT is reduced to a blue formazan product by respiratory enzymes that are active only in viable cells, making the amount of color change indicative of cell

proliferation. Briefly, 2000 cells of each clone (parental, sh-Con, sh-NP2-C8, and sh-NP2-C9) were plated per well in five 96-well microtiter plates in 200 μL of medium. For analysis, 20 μL of MTT substrate (of a 2.5 mg/mL stock solution in phosphate-buffered saline [PBS]) was added to each well, and the plates were returned to standard tissue incubator conditions for an additional 2 hours. Medium was then removed, the cells were solubilized in 200 μL of dimethyl sulfoxide, and colorimetric analysis was performed (wavelength, 570 nm). One plate was analyzed immediately after the cells adhered (approximately 4 hours after plating), and the remaining plates were assayed every 24 hours for the next 4 consecutive days.

Annexin V Staining

To determine the role of NRP2 in mediating survival of HCT-116 cells under conditions of hypoxic stress, cells with normal levels of NRP2 (parental and sh-Con) and reduced levels of NRP2 (sh-NP2-C8 and sh-NP2-C9) were subjected to hypoxic conditions (1% O_2, 99% N_2) for 6 and 24 hours. The relative percentage of apoptotic cells was assessed at these time points using the Annexin V-FITC apoptosis Detection Kit-1 (BD Pharmingen, San Diego, CA) according to the manufacturer's protocol. Annexin V quantitation was performed using a Coulter EPICS XL-MCL fluorescent-activated cell analyzer (Beckman Coulter, Miami, FL) equipped with System II software (Beckman Coulter).

Migration and Invasion Assays

Migration assays were conducted as described previously (18) with minor modifications. Equal numbers (30 000) of control cells (sh-Con) or cells with reduced NRP2 expression (sh-NP2-C8 and sh-NP2-C9) were suspended in 0.5 mL of medium and placed in the top compartment of a standard 8-μm pore Boyden chamber with 0.5 mL of medium added to the bottom compartment. Following 12-hour incubation under standard conditions (37°C/5% CO_2), nonmigrating cells were scraped from the top compartment and cells that had migrated to the bottom compartment were fixed and stained using the Protocol HEMA 3 stain set (Fisher Scientific, Pittsburgh, PA). Membranes were excised and mounted on a standard microscope slide (Curtis Matheson Scientific, Houston, TX). The numbers of migrated cells were determined from 5 random fields visualized at ×20 magnification.

Invasion assays used identical methods, except that the cells were placed in the top compartment of a modified Boyden chamber with a Matrigel-coated membrane. The numbers of invasive cells were determined from five random fields visualized at ×20 magnification.

Soft Agar Colony-Forming Assay

To determine the effect of NRP2 expression on anchorage-independent growth, 6-well plates were coated with 1 mL of medium with 0.8% agarose per well, and 500 cells of each clone (sh-Con, sh-NP2-C8, and sh-NP2-C9) in 1 mL of medium containing 0.5% agarose were added to the wells. Cells were incubated at standard conditions for 12 days (37°C, 5% CO_2). Colonies that were more than 50 μm in diameter were counted under a light microscope at ×20 magnification. For each cell type, five fields were counted, and numbers of colonies are expressed as mean with 95% confidence intervals (CI).

Preparation of siRNA-Containing Liposomes

For experiments to test the efficacy of in vivo therapeutic targeting of NRP2 in tumor xenografts in mice, liposomes containing siRNAs were prepared as previously described (19). Briefly, siRNA oligonucleotides (without hairpins) to NRP2 target sequences (NP2-#1 and NP2-#2) or scrambled control sequences (CON-#1 and CON-#2) were mixed with 1,2-dioleoyl-sn-glycero-3-phosphatidylcholine (DOPC) (Avanti Polar Lipids, Alabaster, AL) at a ratio of 10:1 (w/w) DOPC/siRNA and lyophilized. Immediately before in vivo administration, lyophilized preparations were hydrated in 0.9% saline at a concentration of 5 μg of siRNA per 200 μL and were purified by separating free siRNA from liposomes with filter units with a size exclusion limit of 30 000 Daltons (Millipore Corp).

In Vivo Modeling

Male athymic nude mice, 6–8 weeks old, were purchased from the National Cancer Institute–Frederick Cancer Research Facility (Frederick, MD) and maintained under specific pathogen-free conditions. All animal experiments met the requirements of the MDACC Animal Care Facility and the National Institutes of Health (NIH) guidelines on animal care and use. Each HCT-116 clone was inoculated into mice (10 per group) as previously described (18). In brief, 1.0×10^6 cells (sh-Con, sh-NP2-C8, or sh-NP2-C9) were injected in 0.1 mL of Hanks balanced salt solution per mouse, either subcutaneously (right rear flank) or into the spleen of each nude mouse. Tumor growth was monitored, and at 21–32 days, when three mice in any group become moribund (as judged by lethargy, decreased grooming, and/or weight loss) or had palpable tumors approximately 1 cm in diameter, the mice were killed by CO_2 asphyxia, and final tumor mass and volume were recorded. Tumor volume was calculated as [(length/2) × (width^2)].

For the in vivo siRNA delivery experiments, we created colon cancer cells that expressed the lenti-luc reporter gene by infecting parental HCT-116 cells with a recombinant lentivirus as previously described (20). Luciferase-expressing HCT-116 cells (1.0×10^6 cells per mouse) were suspended in 0.1 mL of Hanks balanced salt solution and inoculated directly into the liver of each mouse (20 mice in total). Four days later, 10 mice were treated with either control- or NRP2-siRNA/liposomal complexes (5 μg siRNA per injection), which were administered intraperitoneally as a 200 μL bolus. Treatments continued every 5 days thereafter for a total of six treatments per group. At 32 days, mice were killed by CO_2 asphyxia, and total body weight, liver weight, and tumor volumes were calculated. Tumor specimens from each treatment group were snap frozen and fixed in formalin or frozen in optimum cutting temperature solution (OCT).

Histopathologic Analysis and Immunohistochemical Staining of Tissues

Patient tissue specimens were analyzed as previously described (21) with an anti-NRP2 antibody (C-9; Santa Cruz Biotechnology, 1:500 dilution). Tumor xenografts from mice were fixed in 10% neutral formalin and paraffin or OCT solution (Miles, Elkhart, IN). Immunostaining was performed according to standard procedures (22,23). Immunofluorescent staining for NRP2 in OCT-embedded xenografts was performed with a rabbit anti-NRP2 antibody (H-300, Santa Cruz Biotechnology, 1:200 dilution), which recognizes human, rat, and mouse NRP2, followed by anti-rabbit fluorescent-conjugated

antibody (Alexa 488, dilution 1:1000) and counterstained with the DNA-specific dye Hoechst 33345 (both from Molecular Probes, Eugene, OR). Stained tissue sections were analyzed with NIH Image J 1.34 software. A minimum of five randomly selected fields or images were examined in all analyses. Fluorescently labeled cells were examined using a Nikon Microphot-FXA fluorescent microscope and representative images recorded.

Bioluminescence Imaging

In vitro and in vivo bioluminescence imaging of luciferase-expressing HCT-116 cells was conducted as previously described (20) using a cryogenically cooled IVIS 100 imaging system coupled to a data-acquisition personal computer equipped with Living Image software (all from Xenogen Corp, Hopkinton, MA). For in vitro imaging, 25 μL of luciferase potassium salt solution (15 mg/mL in PBS) (Sigma-Aldrich) was added to each well of a 12-well plate containing 25 000 HCT-116 cells per well. For in vivo studies, nude mice were anesthetized with a 1.5% isofluorane-oxygen mixture and injected intraperitoneally with luciferase potassium salt solution (15 mg/mL in PBS) at a dose of 150 mg/kg body weight before each imaging session. Initial in vivo images at day 3 were obtained to establish baseline tumor volume as measured by photon emission representative of luciferase activity. Additional images were obtained at 14 and 28 days after inoculation to monitor tumor growth kinetics.

Statistical Analyses

Data are presented as means and as differences in means with 95% confidence intervals for the differences. For the in vitro and in vivo studies, statistical significance was determined by using Fisher exact tests (comparison of incidence) or Mann-Whitney tests (comparison of means), as indicated. For the in vivo experiments, 10 mice in each group were used, as directed by power analysis to detect a 50% reduction in tumor size or weight, with a beta error of 3%. Because sample size was small and outcome variables could have a skewed distribution, the non-parametric Mann-Whitney test was used, and on that basis, 95.7% confidence intervals were iterated. All statistical tests were two-sided, and P values less than .05 were considered to be statistically significant.

Results

Expression of NRP2 in Human Colon Tissues and Cell Lines

We first examined the expression of NRP2 protein in paraffin-embedded samples of human primary colon tumors, adjacent normal colonic mucosa, and colon cancer liver metastases by immunoperoxidase staining (Fig. 1, A). NRP2 protein was not detectable in nonmalignant mucosa (0 [0%] of 10 specimens) but was evident in 10 (83%) of 12 adjacent adenocarcinomas (P = .001 vs nonmalignant mucosa) and five (71%) of seven liver metastases (P = .003 vs nonmalignant mucosa). NRP2 protein was also detected in the Geo, HCT-116, HT-29, KM-12, and SW480 colorectal cancer cell lines. Geo, HCT-116, and SW480 cells expressed the highest levels (Fig. 1, B).

Effect of NRP2 siRNA on NRP2 Levels in Human and Murine Cell Lines

We next examined the effect of using targeted shRNAs to reduce NRP2 levels in human HCT-116 colorectal cancer cells. Specificity

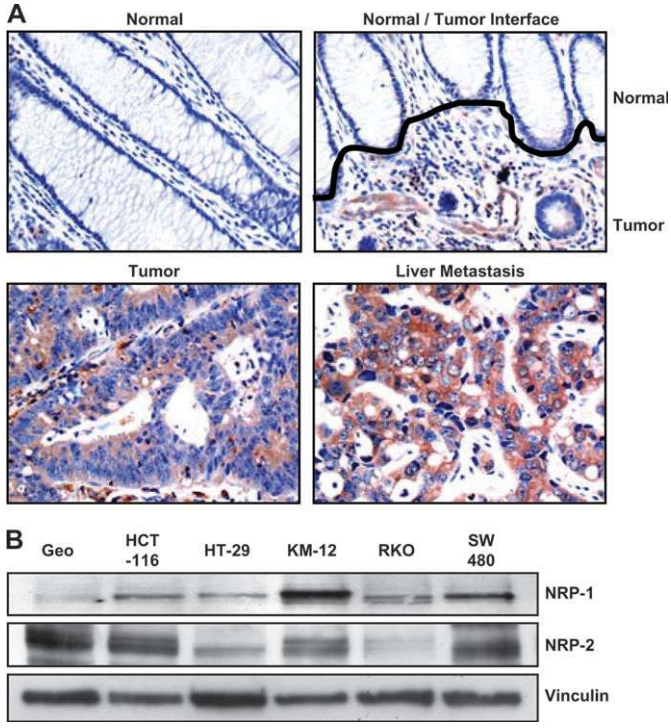

Fig. 1. Assessment of NRP2 expression in human colon tissues and cell lines. (**A**) Representative tissue sections (×20 magnification) of nonmalignant human colonic mucosa (Normal), adjacent colon adenocarcinoma (Normal/Tumor Interface), colon adenocarcinoma (Tumor), and Liver Metastasis stained for expression of NRP2 protein (**brown**). (**B**) Immunoblot analysis of NRP1 and NRP2 expression in six colon adenocarcinoma cell lines. Immunostaining for vinculin was used as an internal loading control.

of siRNA targeting for NRP2 was first confirmed by immunoblot analysis of NRP1 and NRP2 levels in control human HCT-116 cells and cells that had been transfected with control or NRP2 siRNAs (Fig. 2, A, top panel). To further examine specificity of the human NRP2 siRNA sequence for human NRP2, human SW480 colorectal cancer cells and B16BL6 melanoma cells were transiently transfected with increasing concentrations of human NRP2 siRNA (NP2-#1 plus NP2-#2) (Fig. 2, A, bottom panel). The expression of NRP2 was strongly suppressed in human cells transfected with 10 μg of siRNA, but NRP2 expression remained unchanged in transfected B16BL6 mouse cells.

Effect of NRP2 Expression on Cell Proliferation Rates In Vitro

We next used an MTT assay to determine the effect of reduced NRP2 expression on colorectal cancer cell growth rates in vitro. HCT-116 cells stably transfected with shRNA to NRP2 showed no changes in proliferation rate relative to that of parental and sh-Con-transfected HCT-116 cells (Fig. 2, B). Doubling times were approximately 25 hours for both the parental and the sh-Con control cells and 24–26 hours for sh-NP2-C8 and sh-NP2-C9 cells. VEGF-A (10 μg/mL) treatment did not alter the doubling times of any of these cell lines, regardless of NRP2 expression level, compared with doubling times in the absence of VEGF-A (data not shown).

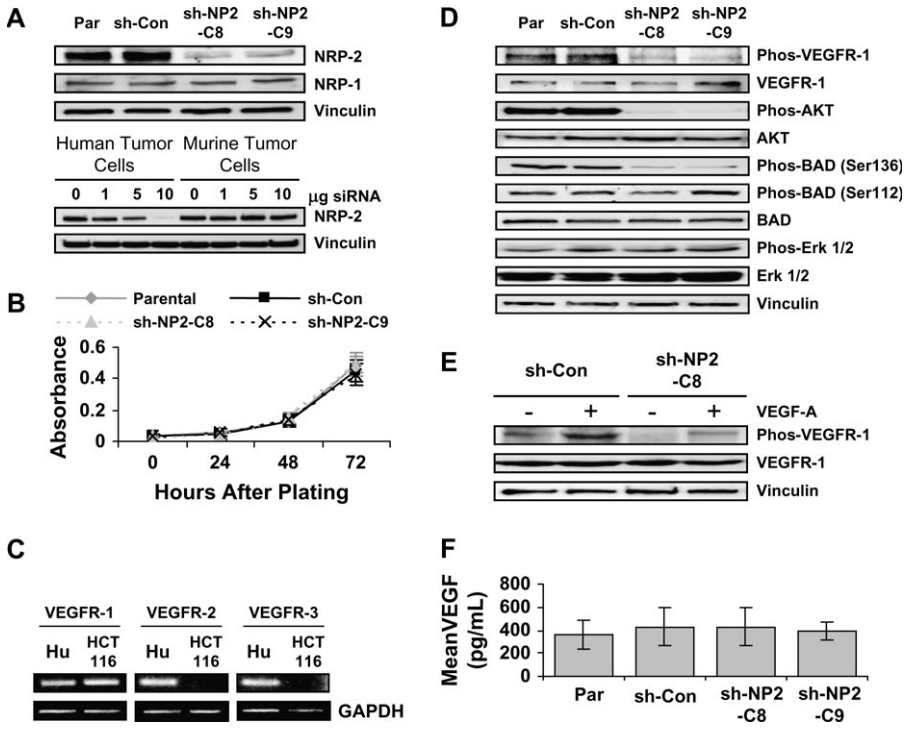

Fig. 2. Effect of NRP2 expression on proliferation and VEGFR1 receptor phosphorylation in HCT-116 cells. (**A**) Creation of stable cell lines with reduced NRP2 levels using shRNAs. **Upper panel**: Immunoblot analysis of NRP2 levels in parental HCT-116 cells carrying no shRNA, control shRNA (sh-Con) or shRNA to NRP2 (sh-NP2-C8 and sh-NP2-C9). **Lower panel**: Immunoblot analysis following transient transfections with increasing concentrations of siRNAs to NRP2 demonstrating specificity of this siRNA for reducing NRP2 levels in human tumor cells (SW480) but not murine cells (murine melanoma cell line B16BL6). (**B**) MTT analysis of growth rates of control cells (parental, sh-Con) or cells with reduced NRP2 expression (sh-NP2-C8, sh-NP2-C9). **Bars** indicate mean of 12 replicates with 95% confidence intervals (CIs). (**C**) Reverse transcriptase-polymerase chain reaction analysis of VEGFR1, VEGFR2, and VEGFR3 expression in HCT-116 cells. Human umbilical vein endothelial cells (Hu) were used as a positive control for expression of all three receptors. Glyceraldehyde 3-phosphate dehydrogenase (GAPDH) was used as a positive control to ensure the integrity of RNA. (**D**) Immunoblot analysis of VEGFR1 pathway activation. Antibodies are used to compare VEGFR1, Akt, and Erk-1/2 and BAD protein levels with phosphorylated protein levels in parental and control shRNA-containing cells and the two NRP2 shRNA–expressing cell lines. Membranes were reprobed with an antibody against vinculin as a loading control. (**E**) Immunoblot analysis showing phosphorylated VEGFR1 levels in control shRNA-carrying cells (sh-Con) and NRP2 shRNA–expressing cells (sh-NP2-C8) grown in serum-reduced media with or without stimulation with VEGF-A (10 μg/mL). Membranes were reprobed with an antibody against vinculin as a loading control. (**F**) Enzyme-linked immunosorbent assay of VEGF expression in culture supernatants from parental cells and NRP2 shRNA-expressing cells. Data are means of three replicates with 95% CIs.

Effect of NRP2 Expression on VEGFR1 and Akt Signaling

NRP2 can act as a coreceptor for VEGFR1, VEGFR2, and VEGFR3 (24,25). HCT-116 cells, like other colon cancer cells (26), express only one of the three known VEGF tyrosine kinase receptors, VEGFR1 (Fig. 2, C). NRP2-mediated activation of any of the VEGF receptors would be expected to result in phosphorylation of the coexpressed VEGFRs and activation of its downstream tyrosine kinase substrates. We used immunoblot analysis to examine whether loss of NRP2 expression was associated with changes in VEGFR1 receptor phosphorylation. NRP2 shRNA–expressing cells showed no change in VEGFR1 levels but did show a substantial reduction in VEGFR1 phosphorylation compared with levels in control sh-Con and parental cells (Fig 2, D). Examination of the activation of downstream signaling intermediates using immunoblots probed with phospho-specific antibodies showed that loss of NRP2 also led to substantial reductions in the phosphorylation of Akt and the downstream antiapoptosis protein BAD (Ser136), whereas the phosphorylation of Erk-1/2 remained unchanged (Fig. 2, D). To confirm the effects of decreased NRP2 expression on downstream pathways, we studied signaling intermediates in a second colorectal cancer cell line (SW480) after transient transfection with NRP2 siRNAs. Transient reduction of NRP2 levels by siRNA in SW480 cells also led to decreased Akt phosphorylation (without altering the levels of Erk-1/2 phosphorylation; data not shown).

To examine whether the loss of VEGFR1 phosphorylation accompanying reduced NRP2 levels in HCT-116 cells could be overcome by the addition of exogenous VEGF-A, control cells and NRP2 shRNA–expressing cells were grown in serum-reduced medium (1% fetal calf serum) and stimulated with VEGF-A (10 μg/mL) for 10 minutes, followed by protein extraction and immunoblot analysis. In agreement with the pattern shown in Fig. 2, D, basal phosphorylation of VEGFR1 was lower in cells with reduced NRP2 levels (Fig. 2, E). VEGFR1 phosphorylation was increased upon VEGF-A–stimulation in control cells to a greater extent than in HCT-116 transfectants with shRNA-mediated reduction of NRP2 levels.

Effect of NRP2 Expression on Endogenous Expression of VEGF-A and Sema3F

To determine whether the changes in VEGFR1 phosphorylation observed in the NRP2 shRNA-expressing cells had resulted from potential changes in NRP2 ligand expression, we next examined levels of VEGF-A and Sema3F in HCT-116 cells with varying levels of NRP2 expression. VEGF-A levels, as determined by ELISA, were nearly the same in parental and sh-Con cells and in both clones with suppressed NRP2 expression (sh-NP2-C8 and sh-NP2-C9). Immunoblot analysis of control and NRP2 siRNA–expressing cells showed that levels of Sema3F expression were the same in all of these lines (data not shown).

Effect of NRP2 Expression on Anchorage-Independent Growth of Colon Cancer Cells

On the basis of our finding that NRP2 gene silencing was associated with reduced phosphorylation of antiapoptosis proteins, we next assessed the effect of NRP-2 expression on growth of colon

cancer cells under anchorage-independent conditions. Control cells (sh-Con) formed abundant large (>50 μm in diameter) colonies in soft agar, whereas cells with reduced levels of NRP2 formed statistically significantly fewer colonies in soft agar, and the colonies that did form were generally smaller than those derived from control cells (Fig. 3, A and B; mean number of colonies: sh-Con = 384, sh-NP2-C8 = 112, sh-NP2-C9 = 81; sh-NP2-C8 vs control: difference = 272 colonies, 95% CI = 210 to 334 colonies, $P = .002$; sh-NP2-C9 vs sh-Con control: difference = 303 colonies, 95% CI = 253 to 353 colonies, $P = .002$).

Effect of NRP2 Expression on Colon Cancer Cell Survival During Hypoxia

To further investigate the mechanism by which reduced expression of NRP2 altered survival of colorectal cancer cells, HCT-116 cells with normal and reduced levels of NRP2 were subjected to normoxic or hypoxic growth conditions (1% O_2, 99% N_2), and the relative percentages of Annexin V–staining cells were quantified as a measure of apoptosis. Under normoxic conditions, no discernable difference in constitutive apoptotic rates was detected between the two cell types. However, after 6 hours and 24 hours of exposure to hypoxic conditions, cells with decreased NRP2 expression demonstrated a statistically significant increase in apoptosis (Fig. 3, C; at 6 hours of hypoxia, mean sh-Con apoptotic rate = 1.46%, mean sh-NP2-C8 rate = 2.94%, difference = 1.48%, 95% CI = 1.11 to 1.85%, $P = .01$; at 24 hours of hypoxia mean sh-Con apoptotic rate = 1.96%, mean sh-NP2-C8 rate = 3.52%, difference = 1.56%, 95% CI = 0.98 to 2.14%, $P = .008$).

Effect of NRP2 on Migration and Invasion

VEGFR1 activity has previously been shown to mediate tumor cell migration and invasion (27–29). Our observation that loss of NRP2 expression reduced VEGFR1 phosphorylation and activation of the VEGFR1 pathway led us to assess the effects of NRP2 on the migration and invasion capabilities of colorectal cancer cells with the use of standard and Matrigel-coated Boyden chamber assays, respectively. NRP2 shRNA-expressing cells displayed statistically significantly reduced migration compared with control cells (Fig. 4, A, B; mean cell migration for parental = 187 cells, sh-Con = 167 cells, sh-NP2-C8 = 91 cells, sh-NP2-C9 = 64 cells; sh-NP2-C8 vs sh-Con: difference = 76 cells, 95% CI = 48 to 104 cells, $P = .008$; sh-NP2-C9 vs sh-Con: difference = 103 cells, 95% CI = 73 to 133 cells, $P = .008$). In Matrigel invasion assays, clones with reduced NRP2 levels showed reduced invasiveness compared with controls (Fig. 4, C, D; mean invasion for parental = 83 cells, mean sh-Con = 89 cells, mean sh-NP2-C8 = 44 cells; mean sh-NP2-C9 = 29 cells; sh-NP2-C8 vs sh-Con: difference = 45 cells, 95% CI = 30 to 60 cells, $P = .008$; sh-NP2-C9 vs sh-Con: difference = 60 cells, 95% CI = 44 to 76 cells, $P = .008$). To examine the effect of VEGF-A stimulation on cell migration in cells with decreased NRP2 levels, sh-Con and sh-NP2-C8 cells were grown in serum-reduced medium (1% fetal calf serum) and stimulated with VEGF-A (10 μg/mL) for 24 hours. Although migration was higher in each VEGF-A–treated cell line compared with untreated cells, cells with reduced NRP2 levels (sh-NP2-C8) migrated less in response to VEGF-A stimulation than cells with normal levels of NRP2 (sh-Con) (data not shown).

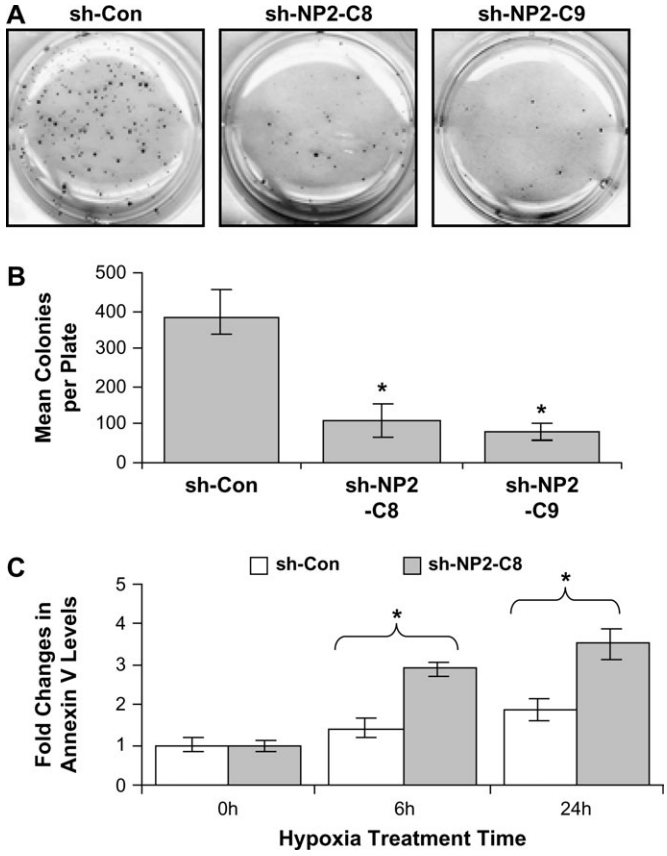

Fig. 3. Effect of NRP2 expression on survival or apoptosis of colorectal cancer cells in vitro (**A**) Representative images of soft agar assay of a well from control cells and cells with reduced NRP2 levels (magnification × 0.75). Growth of control HCT-116 cells (sh-Con) and HCT-116 cells with reduced NRP2 expression (sh-NRP2-C8 and sh-NP2-C9) in soft agar. Cells were plated at low density in medium containing 0.5% agarose, and colonies larger than 50 μm in diameter were counted 14 days later. Large colonies appearing in representative wells containing control cells (sh-Con) or cells expressing NRP2 shRNA (sh-NP2-C8, sh-NP2-C9) are shown. (**B**) Graphical representation of soft agar assay. Viable colonies in three wells were counted, and values are means with 95% confidence intervals (CIs). All soft agar assays were performed in duplicate. **Asterisks** indicate statistically significant differences in NRP2 shRNA–containing cells compared with controls (mean sh-Con = 384 colonies, 95% CI = 340 to 428 colonies; mean sh-NP2-C8 = 112 colonies, 95% CI = 69 to 155 colonies, $P = .002$ vs sh-Con control; and mean sh-NP2-C9 = 81 colonies, 95% CI = 56 to106 colonies, $P = .002$ vs sh-Con control). (**C**) Graphical representation of Annexin V apoptosis detection assay. HCT-116 cells were either untreated or subjected to hypoxia (1% O_2) for 6 hours and 24 hours, and the percent of apoptotic cells was determined. Values are means five replicates with 95% CIs. **Asterisks** indicate statistically significant differences in NRP2 shRNA–containing cells vs controls (sh-Con 6 h hypoxia mean = 1.42%, 95% CI = 1.22% to 1.69%, mean sh-NP2-C8 6 h hypoxia = 2.9%, 95% CI = 2.75% to 3.12%, $P = .01$ vs sh-Con 6h hypoxia, mean sh-Con 24 h hypoxia = 1.96%, 95% CI = 1.68% to 2.24%, mean sh-NP2-C8 24 h hypoxia mean = 3.52%, 95% CI = 3.13% to 3.91%, $P = .008$ vs sh-Con 24 h hypoxia).

Effect of NRP2 Expression on Tumor Growth In Vivo

To examine the effect of NRP2 expression on tumor growth, we injected equal numbers (1.0×10^6 per mouse) of HCT-116 control cells (sh-Con) or NRP2 siRNA-expressing cells (sh-NP2-C8 and sh-NP2-C9) subcutaneously into nude mice (groups of 10) and assessed tumor incidence and volume 30 days later. All mice were of approximately the same overall weight when killed. Tumor incidence was 100% in control (sh-Con) mice, 40% in sh-NP2-C9

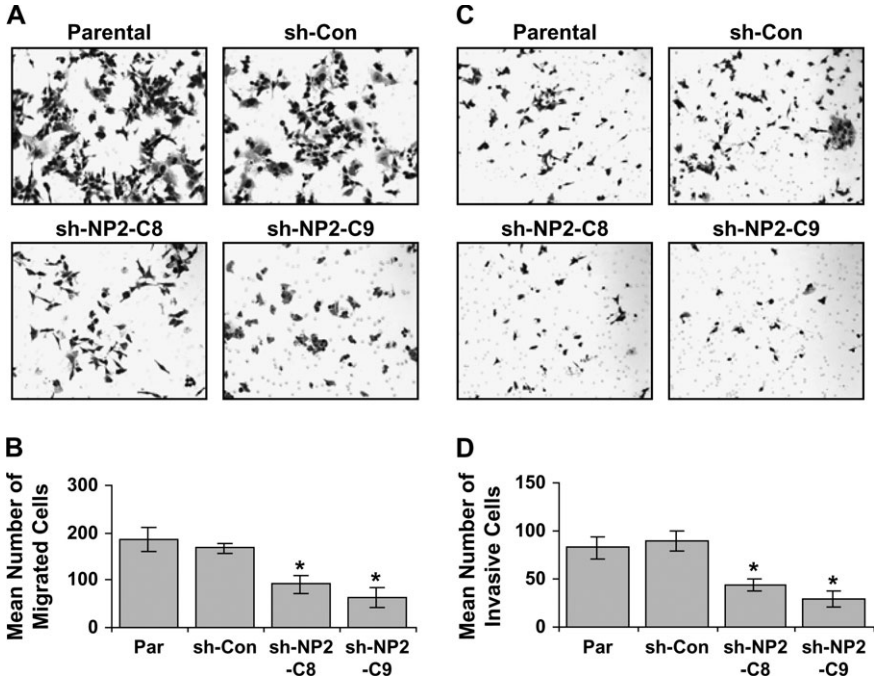

Fig. 4. Effect of NRP2 expression on migration and invasion by colorectal cancer cells. (**A**) Representative images (×20) of migration assays of colon cancer cells with normal levels of NRP2 expression (parental and sh-Con) and cells with suppressed levels of NRP2 expression (sh-NP2-C8 and Sh-NP2-C9). (**B**) Mean number of cells from five independent assays that migrated in (**A**). **Asterisks** indicate statistically significant differences in NRP2 shRNA-containing cells vs sh-Con control. Mean parental = 187 cells, 95% confidence interval (CI) = 157 to 217 cells; mean sh-Con = 167 cells, 95% CI = 152 to 182 cells; mean sh-NP2-C8 = 91, 95% CI = 67 to 115 cells, P = .008 vs sh-Con; and mean sh-NP2-C9 = 64 cells, 95% CI = 39 to 89 cells, P = .008 vs sh-Con. (**C**) Invasion assay of parental HCT-116 cells, sh-Con cells, sh-NP2-C8, and sh-NP2-C9 cells in modified Boyden chambers with Matrigel-coated membrane, in which 30 000 cells of each clone were plated, and, after 12 hours, invasive cells which had digested and moved through the matrigel membrane were stained and counted under a microscope (×20 magnification). (**D**) Graphical representation of invasive cells calculated as mean value ± 95% CI from five fields at ×20 magnification. **Asterisks** indicate statistically significant differences in NRP2 shRNA–containing cells vs sh-Con. Mean parental = 83 cells, 95% CI = 69 to 97 cells; mean sh-Con = 89 cells, 95% CI = 76 to 102 cells; mean sh-NP2-C8 = 44 cells, 95% CI = 36 to 52 cells, P = .008 vs sh-Con; mean sh-NP2-C9 = 29 ± 5 cells, 95% CI =19 to 39 cells, P = .008 vs sh-Con.

mice, and 60% in sh-NP2-C9 mice (Fig. 5, A). Subcutaneous tumors produced by cells with reduced NRP2 expression were statistically significantly smaller than those produced by control cells expressing normal levels of NRP2 (sh-Con) (Fig. 5, B; mean volume sh-Con = 1.0 cm^3, sh-NP2-C8 = 0.1 cm^3, sh-NP2-C9 = 0.2 cm^3; sh-NP2-C8 vs control: difference = 0.9 cm^3, 95% CI = 0.7 to 1.2 cm^3, P = .01; sh-NP2-C9 vs control: difference = 0.8 cm^3, 95% CI = 0.5 to 1.1 mm^3, P = .01).

To examine the effect of NRP2 expression on hepatic metastasis of HCT-116 colorectal cancer cells, equal amounts of cells (1.0×10^6 per mouse) of each clone were inoculated into the spleens of nude mice (groups of 10) and the resulting liver metastases were counted and measured 30 days later. The incidence of hepatic metastases was lower in the mice inoculated with NRP2 siRNA-expressing cells than in the mice injected with control cells (Fig. 5, A; mean sh-Con = 100%, mean sh-NP2-C8 = 20%, mean sh-NP2-C9 = 40%, sh-NP2-C8 vs sh-Con control: difference = 80%, 95% CI = 44% to 97%, P = .002; sh-NP2-C9 vs sh-Con control: difference = 60%, 95% CI = 26% to 88%, P = .01). Analysis of mice that developed hepatic metastases revealed that inoculation with cells with reduced NRP2 expression resulted in fewer hepatic metastases than inoculation with cells with normal levels of NRP2 (Fig. 5, C; mean sh-Con = 19 metastases, mean sh-NP2-C8 = 1 metastasis, mean sh-NP2-C9 = 6 metastases; sh-NP2-C8 vs sh-Con control: difference = 18 metastases, 95.7% CI = 3 to 50 metastases, P < .001, as determined by Mann-Whitney analysis; sh-NP2-C9 vs sh-Con control: difference = 13 metastases, 95.7% CI = 2 to 48 metastases, P = .006, as determined by Mann-Whitney analysis). In addition, the final volumes of the metastases that did form were smaller for NRP2 shRNA-expressing cells (sh-NP2-C8 and sh-NP2-C9) than for shRNA control cells (Fig. 5, D and E; mean sh-Con = 79 mm^3, mean sh-NP2-C8 = 1 mm^3, mean sh-NP2-C9 = 9 mm^3; sh-NP2-C8 vs control: difference = 78, 95.7% CI = 1.1 to 69 mm^3, P < .001, as determined by Mann-Whitney analysis; sh-NP2-C9 vs sh-Con control: difference = 70 mm^3, 95.7% CI = 1.1 to 69 mm^3, P = .004, as determined by Mann-Whitney analysis).

NRP2 Expression and Apoptosis In Vivo

To examine the effect of NRP2 expression on apoptosis in vivo, we stained xenograft tissue samples derived from the sh-Con, sh-NP2-C8, and sh-NP2-C9 cell lines for Annexin V. Tumors with reduced NRP2 expression exhibited 5–10 times more apoptotic cells per ×20 field than did the control tumors (Fig. 6; mean sh-Con control = 4 apoptotic cells, mean sh-NP2-C8 = 24 apoptotic cells, mean sh-NP2-C9 = 36 apoptotic cells, sh-NP2-C8 vs sh-Con control: difference = 20 apoptotic cells, 95% CI = 5 to 35 apoptotic cells, P = .01 vs sh-Con; sh-NP2-C9 to sh-Con control: difference = 32 apoptotic cells, 95% CI = 18 to 45 apoptotic cells, P = .005).

Effect of In Vivo Targeting of NRP2 on Colon Cancer Progression

To determine whether siRNAs to NRP2 might be used to treat human tumors (ie, tumors derived from untransfected cells), we explored the use of liposomes carrying NRP2 siRNA to target tumor xenografts in mice. Before targeting NRP2 expression in vivo, we first tested whether siRNA incorporated into liposomes made of the neutral lipid DOPC (19) could effectively reduce gene expression in tumors growing in the murine liver. For these experiments, luciferase-specific siRNA, which we had confirmed was effective in attenuating luciferase activity in vitro (Fig. 7, A, top), was complexed with DOPC and injected intraperitoneally into mice at a dose of 5 μg per mouse 10 days after the inoculation of 1.0×10^6 HCT-116 colon cancer cells expressing the lenti-luc gene.

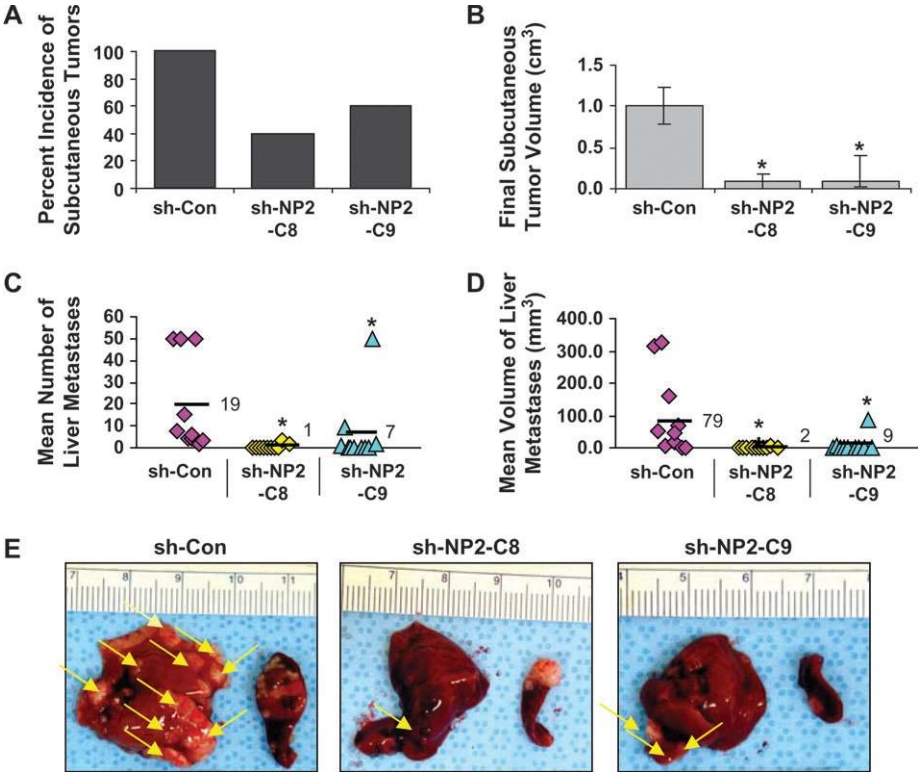

Fig. 5. Effect of NRP2 expression on in vivo growth and metastasis of colorectal cancer cells. (**A**) Tumor incidence in 10 nude mice per group 30 days after subcutaneous injection with control (sh-Con) HCT-116 cells or with HCT-116 cells with reduced NRP2 expression (sh-NP2-C8 and sh-NP2-C9). (**B**) Final tumor volumes 30 days after subcutaneous injection of stable clones of HCT-116 cells expressing control shRNA or shRNAs to reduce NRP2 expression. Data are means with 95% confidence intervals (CIs) from 10 mice. **Asterisks** indicate statistically significant differences between NRP2 shRNA–containing cells vs sh-Con cells. Mean volume sh-Con = 1.0 cm^3, 95% CI = 0.8 to 1.2 cm^3; mean volume sh-NP2-C8 = 0.1 cm^3, 95% CI = 0 to 0.2 cm^3, $P = .01$ vs sh-Con; mean sh-NP2-C9 = 0.2 cm^3, 95% CI = 0.0 to 0.4 cm^3, $P = .01$ vs sh-Con. (**C**) Scatter plot analyses of final numbers of liver metastases 30 days after intrasplenic injection of stable clones of HCT-116 cells expressing control shRNA or shRNAs to reduce NRP2 expression. **Bars** indicate average value. **Asterisks** indicate statistically significant differences for sh-NP-C8 ($P < .001$) and sh-NP-C9 ($P = .006$) vs sh-Con (as determined by Mann-Whitney analysis). (**D**) Scatter plot analyses of final volumes of the combined hepatic metastases from ten mouse 30 days after intrasplenic injection of control cells or cells with reduced NRP2 expression. **Bars** indicate average value. **Asterisks** indicate statistically significant differences for sh-NP2-C8 ($P < .001$) and sh-NP2-C9 ($P = .004$) vs sh-Con (as determined by Mann-Whitney analysis). (**E**) Photographs of excised livers and spleens from mice injected with control cells or NRP2 shRNA-expressing cells. **Arrows** indicate metastases.

The mice were subjected to bioluminescent imaging before siRNA-DOPC administration to establish baseline activity and again 48 hours after siRNA treatment to examine whether administration of siRNA against luciferase in liposomes led to a reduction in luciferase activity in the tumor cells. Hepatic luciferase activity, as reflected by photon emission, was approximately 50% lower in treated mice than in the same mice measured before siRNA-Luc-DOPC administration (Fig. 7, A, bottom).

Finally, we examined the effect of in vivo administration of siRNA to NRP2 in liposomes on the growth and metastasis of colorectal cancer xenografts in nude mice. For these experiments, control siRNA scrambled sequences (Con-#1 and Con-#2) or NRP2 siRNA target sequences (NP2-#1 and NP2-#2) were complexed with DOPC and injected intraperitoneally into mice at a dose of 5 μg per mouse every 5 days, starting 4 days after the direct hepatic inoculation of 1.0×10^6 HCT-116 lenti-luc–transfected colorectal cancer cells per mouse. Bioluminescent imaging of tumor cell growth showed that administration of NRP2 siRNA-DOPC impaired the growth kinetics of colorectal cancer cells compared with those of control cells at 28 days after inoculation (Fig. 7, B; mean control activity = 9.8×10^8 photons, mean NRP2 siRNA-DOPC = 1.7×10^8 photons, NRP2 vs control: difference = 8.1×10^8, 95% CI = 1.3×10^8 to 15.0×10^8, $P < .001$. Livers from the control groups had more tumor volume (Fig. 7, E) than those from mice treated with siRNA to NRP2 (Fig. 7, C: mean control siRNA-DOPC = 420 mm^3, mean NRP2 siRNA-DOPC = 36 mm^3, NRP2 vs control: difference = 384 mm^3, 95% CI = 174 to 595 mm^3, $P = .005$). In addition, the ratios of liver to total body weight were statistically significantly higher in the control group than in the NRP2-treated group (Fig. 7, D: mean control siRNA-DOPC = 0.124; mean NRP2 siRNA-DOPC = 0.067; NRP2 vs control: difference = 0.057, 95% CI = 0.032 to 0.082, $P < .001$).

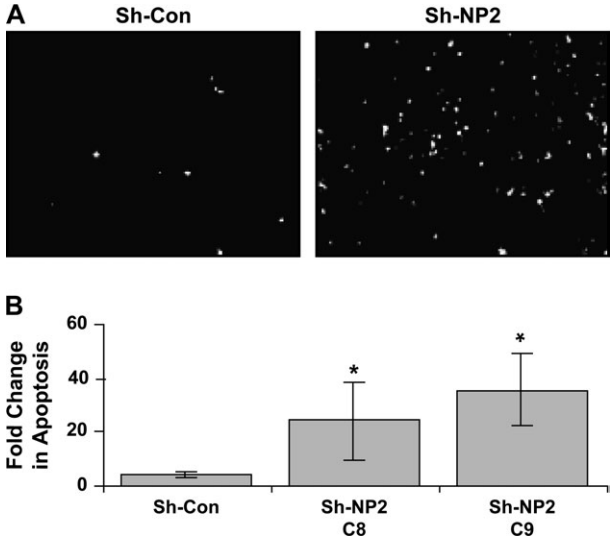

Fig. 6. Effect of NRP2 expression on apoptosis in tumor xenografts. (**A**) Inverted images (×40 magnification) of tumor sections from subcutaneously injected nude mice in Fig. 5 that have been immunofluorescently stained to detect annexin V expression as a measure of the number of apoptotic cells. (**B**) Graphical representation of annexin V staining, calculated with the mean value of the control set as equaling 1.0 **Asterisks** indicate statistically significant differences. Mean sh-Con = 4 apoptotic cells, 95% confidence interval (CI) = 3 to 6; mean sh-NP2-C8 = 24 apoptotic cells, 95% CI = 9 to 39 apoptotic cells, $P = .01$ vs sh-Con; mean sh-NP2-C9 = 36 apoptotic cells, 95% CI = 23 to 49 apoptotic cells, $P = .05$ vs sh-Con.

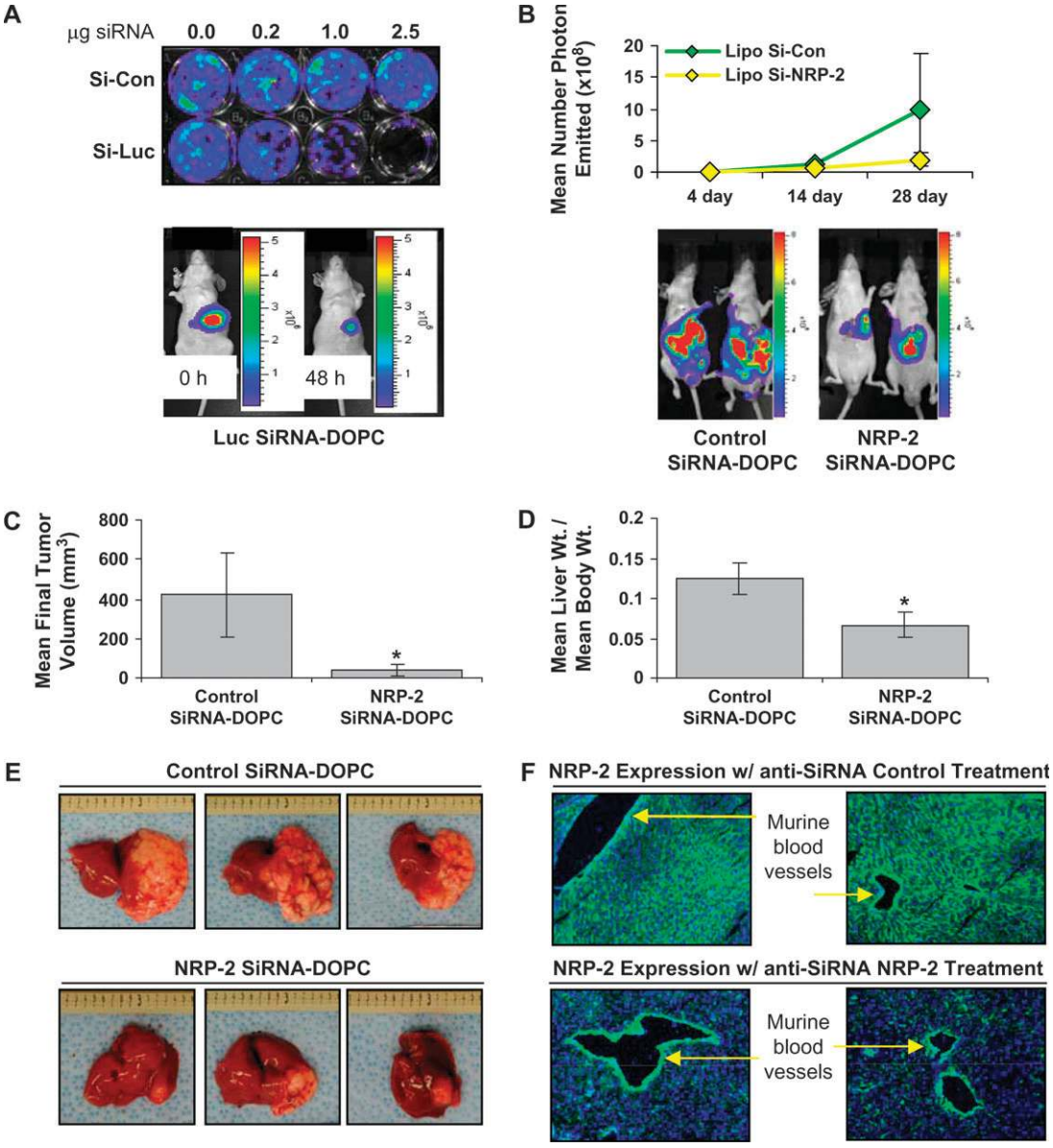

Fig. 7. Effect of administration of liposomal-conjugated siRNA on colorectal tumor growth in vivo. (**A**) **Top**: in vitro assay demonstrating reduced luciferase activity in HCT-116 cells carrying the lenti-luc gene after transient transfection with luciferase siRNA. Twenty-four hours after plating the cells in 12-well dishes, siRNA to luciferase or scrambled control siRNA was transiently transfected at the indicated concentrations. **Bottom**: In vivo luciferase activity in a mouse carrying hepatic tumors after intrahepatic inoculation with 1.0×10^6 HCT-116 cells harboring the lenti-luc gene. Mice were treated with anti–luciferase-siRNA/1,2-dioleoyl-sn-glycero-3-phosphatidylcholine (DOPC) complex (5 μg per mouse at 10 days after tumor cell implantation) and were imaged again at 48 hours after siRNA treatment. The images shown are of a representative single mouse before and after treatment with luciferase siRNA-DOPC. (**B**) **Top**: Plot of average in vivo bioluminescent activity as photon emissions from mice at 3, 14, and 28 days after hepatic inoculation with 1.0×10^6 HCT-116 cells harboring the lenti-luc gene. Data are means with 95% confidence intervals (CIs) from 10 mice treated intraperitoneally at day 4 and every 5 days thereafter with control-siRNA-DOPC complex or NRP2 siRNA-DOPC complex. Day 28 mean control activity = 9.8×10^8 photons, mean NRP2 siRNA-DOPC = 1.7×10^8 photons, NRP2 vs control: difference = 8.1×10^8, $P < .001$ as determined by Mann-Whitney analysis. **Bottom:** Representative images of mouse bioluminescent activity at day 28 in siRNA treatment groups as described above. (**C**) Final tumor volumes from mice in (**B**) at 32 days after inoculation of 1.0×10^6 HCT-116 cells. Mice received six total intraperitoneal injections of liposomal control- or NRP2-specific siRNA complexes (control siRNA; Con-#1 and Con-#1, NRP2 siRNA; NP2-#1 and NP2-#2, a total of 5-ug siRNA per treatment). Final tumor volumes were calculated as [(length/2) × (width^2)] and are presented as means with 95% CIs. **Asterisk** indicates a statistically significant difference in NRP2- vs control siRNA–DOPC. Mean control siRNA-DOPC = 420 mm^3, mean NRP2 siRNA-DOPC = 36 mm^3, NRP2 vs control: difference = 384 mm^3, 95% CI = 174 to 595 mm^3, $P = .005$. (**D**) Final liver weights/ total body weights of mice in (**B**) from in vivo siRNA treatment groups. Values are means with 95% CIs. **Asterisk** indicates a statistically significant difference in liver weights/total body weights from NRP2- vs control siRNA–treated mice. Mean control siRNA-DOPC = 0.124; mean NRP2 siRNA-DOPC = 0.067; NRP2 vs control: difference = 0.057, 95% CI = 0.032 to 0.082, $P < .001$). (**E**) Representative photographs of excised livers from mice in (**B**) treated with either nonspecific or NRP2-targeted siRNA and killed at 32 days after inoculation. (**F**) Representative photographs of immunohistochemical staining of tumors from the mice described above showing the specificity of NRP2 siRNAs for reducing human, and not mouse, NRP2 levels. **Top panels**, section from control (control siRNA-DOPC–treated) tumors showing NRP2 expression (**green fluorescence**) in both human tumor cells and murine endothelial cells. **Bottom panels**, sections from NRP2 siRNA-DOPC–treated tumors showing substantially decreased NRP2 expression in human tumor cells compared with control, whereas NRP2 expression in murine vascular/endothelial cells (**yellow arrows**) remains unchanged. Hoechst staining (**blue**) was used to demarcate nuclei.

Immunohistochemical examination of tumor samples revealed that only human NRP2 expression (in tumor xenografts) and not mouse NRP2 expression (on murine endothelial cells) was decreased in mice treated with NRP2 siRNA-DOPC compared with mice treated with control siRNA-DOPC (Fig. 7, F).

Discussion

Our findings demonstrate that NRP2 is a potential therapeutic target in that its expression is critical for the growth and metastasis of colorectal cancer cells. Specifically, we demonstrated that NRP2 expression was elevated in most of the human primary and metastatic colon cancer specimens tested compared with normal colonic mucosa. We also showed that NRP2 was expressed in most of the human colorectal cancer cell lines tested. Reduction of NRP2 levels by shRNA decreased the phosphorylation and activation of VEGFR1, which, as we have shown here, is the only VEGF tyrosine kinase receptor expressed in HCT-116 colorectal cancer cells. These changes in VEGFR1 activity took place in the absence of changes in levels of the NRP2 ligands VEGF and Sema3F. In addition, we showed that constitutive phosphorylation of the critical intercellular signaling intermediate Akt and the antiapoptosis protein BAD decreased in conjunction with the observed reduction in VEGFR1 activity. Although previous work with endothelial cells suggested that NRP2 can coimmunoprecipitate with VEGFR1 (25), it was unclear whether this association modulated VEGFR1 activity and if it occurs in other cell types. Our findings suggest that NRP2 expression is a critical activator of VEGFR1 in colorectal cancer cells (and potentially in other cell types in which only VEGFR1 is coexpressed with NRP2), possibly by enhancing the stimulation of VEGFR1 by VEGF.

One critical function that has been attributed to VEGF stimulation is the enhanced survival of target cells (30–32), which in some systems has been demonstrated to be dependent on regulation of prosurvival proteins by activation of the PI-3′-kinase/Akt pathway (32,33). VEGFR1 activity has been demonstrated to promote survival in endothelial cells (34). Here, we showed that reduced expression of the VEGF receptor NRP2 makes colorectal cancer cells more susceptible to apoptosis in vitro and in vivo. HCT-116 cells with reduced levels of NRP2 were less capable of surviving under anchorage-independent and hypoxic growth conditions, and tumors derived from HCT-116 cells with reduced NRP2 levels demonstrated increased levels of apoptosis compared with cells that expressed endogenous levels of NRP2. Our in vitro studies showed that loss of NRP2 expression reduces VEGFR1 activity in colorectal cancer cells. Furthermore, NRP2 expression was also required to maintain constitutive phosphorylation of Akt and its downstream target, the antiapoptosis factor BAD, both of which are known to be critical for cell survival (35,36). Our data suggest that NRP2 augments VEGF-mediated survival through VEGFR1/Akt-dependent regulation of these apoptotic mediators.

We also showed that loss of NRP2 reduced the ability of HCT-116 cells to migrate and invade in vitro. A previous report demonstrated that NRP2 mediates motility on endothelial cells, albeit in a VEGFR2/VEGFR3–dependent manner (24). VEGFR1 activation is known to mediate migration of other cell types (27–29). Our findings suggest that NRP2 enhances VEGF-mediated promotion of cell migration and invasion in colorectal cancer cells, presumably through the enhanced activation of VEGFR1, the only VEGFR tyrosine kinase receptor expressed in HCT-116 cells.

We also showed the importance of NRP2 in colon cancer cell growth, both through the use of stable cell lines with reduced NRP2 expression and by in vivo targeting of NRP2 with liposomal-conjugated siRNA. Tumors derived from human colorectal cancer cell lines that lacked expression of NRP2 were less capable of establishing liver metastases in a mouse metastasis model than control tumors with endogenous NRP2 expression. Furthermore, the tumors expressing NRP2 shRNA that did grow, both in the liver and subcutaneously, were smaller than tumors derived from cells with normal levels of NRP2. Similar results were achieved when liposome-conjugated siRNA to NRP2 was used to treat human colon cancer cells implanted in murine liver in vivo.

One potential limitation of this study could be that in vivo siRNA targeting of NRP2 might reduce murine NRP2 expression in addition to human NRP2 expression; thus, the inhibition of the hepatic tumor growth observed may not exclusively be from the reduced expression of the human homolog. However, even though the sequences targeted by the human siRNA used were approximately 80% similar to those in the murine gene, the siRNAs in our studies did not reduce endogenous NRP2 expression in a murine melanoma cell line in vitro. Furthermore, immunohistochemical staining of tumor samples from in vivo siRNA targeting of NRP2 demonstrated that murine endothelial cells retained NRP2 expression, providing further evidence that expression of only the human isoform of NRP2 was reduced by systemic administration of NRP2 siRNA. Additionally, because NRP2 also mediates lymphangiogenesis on lymphatic endothelial cells (37), tumor samples from in vivo targeting were also examined for lymphangiogenesis by staining for the lymphatic endothelial cell maker LYVE-1. No differences were observed in lymphatic vessel content in control siRNA or NRP2 siRNA treatment groups (data not shown). Collectively, these findings suggest that the observed changes in tumor growth and metastasis were mediated through interference with NRP2 function on tumor cells. Lastly, although targeting NRP2 on tumor cells led to a decrease in tumor growth, we cannot state whether this inhibition occurs through interrupting VEGF-dependent or -independent functions. It is unknown whether inhibition of NRP2 signaling may be a mechanism of action of anti-VEGF (bevacizumab) therapy.

In summary, we have shown that NRP2 expression enhances cell survival, migration, invasion, and in vivo tumor growth—all critical aspects of colorectal cancer growth and progression—and our findings suggest that NRP2 may be a promising therapeutic target for colorectal cancer. The use of anti-NRP2 therapeutic targeting in conjunction with anti-VEGF therapy may improve on existing antiangiogenesis treatments and may provide a unique opportunity to circumvent the ability of NRP2-expressing tumors, such as colorectal cancers, to grow and metastasize.

References

1. Folkman J, Shing Y. Angiogenesis. *J Biol Chem.* 1992;267(16):10931–10934.
2. Ferrara N. VEGF and the quest for tumour angiogenesis factors. *Nat Rev Cancer*. 2002;2(10):795–803.

3. Hicklin DJ, Ellis LM. Role of the vascular endothelial growth factor pathway in tumor growth and angiogenesis. *J Clin Oncol*. 2005;23(5): 1011–1027.
4. Ferrara N, Gerber HP, LeCouter J. The biology of VEGF and its receptors. *Nat Med*. 2003;9(6):669–676.
5. Wey JS, Stoeltzing O, Ellis LM. Vascular endothelial growth factor receptors: expression and function in solid tumors. *Clin Adv Hematol Oncol*. 2004;2(1):37–45.
6. Ellis LM. The role of neuropilins in cancer. *Mol Cancer Ther*. 2006;5(5):1099–1107.
7. Bielenberg DR, Pettaway CA, Takashima S, Klagsbrun M. Neuropilins in neoplasms: expression, regulation, and function. *Exp Cell Res.* 2006; 312(5):584–593.
8. Karpanen T, Heckman CA, Keskitalo S, et al. Functional interaction of VEGF-C and VEGF-D with neuropilin receptors. *FASEB J*. 2006; 20(9):1462–1472.
9. He Z, Tessier-Lavigne M. Neuropilin is a receptor for the axonal chemorepellent semaphorin III. *Cell.* 1997;90(4):739–751.
10. Chen H, Chedotal A, He Z, Goodman CS, Tessier-Lavigne M. Neuropilin-2, a novel member of the neuropilin family, is a high affinity receptor for the semaphorins Sema E and Sema IV but not Sema III. *Neuron*. 1997;19(3):547–559.
11. Fuh G, Garcia KC, de Vos AM. The interaction of neuropilin-1 with vascular endothelial growth factor and its receptor flt-1. *J Biol Chem.* 2000;275(35):26690–26695.
12. Whitaker GB, Limberg BJ, Rosenbaum JS. Vascular endothelial growth factor receptor-2 and neuropilin-1 form a receptor complex that is responsible for the differential signaling potency of VEGF(165) and VEGF(121). *J Biol Chem.* 2001;276(27):25520–25531.
13. Lee P, Goishi K, Davidson AJ, Mannix R, Zon L, Klagsbrun M. Neuropilin-1 is required for vascular development and is a mediator of VEGF-dependent angiogenesis in zebrafish. *Proc Natl Acad Sci USA*. 2002;99(16):10470–10475.
14. Wang L, Zeng H, Wang P, Soker S, Mukhopadhyay D. Neuropilin-1-mediated vascular permeability factor/vascular endothelial growth factor (VPF/VEGF)-dependent endothelial cell migration. *J Biol Chem.* 2003;278(49):48848– 48860.
15. Pan Q, Chanthery Y, Liang WC, et al. Blocking neuropilin-1 function has an additive effect with anti-VEGF to inhibit tumor growth. *Cancer Cell.* 2007;11(1):53–67.
16. Hong TM, Chen YL, Wu YY, et al. Targeting neuropilin 1 as an antitumor strategy in lung cancer. *Clin Cancer Res.* 2007;13(16):4759–4768.
17. Gray MJ, Zhang J, Ellis LM, et al. HIF-1alpha, STAT3, CBP/p300 and Ref-1/APE are components of a transcriptional complex that regulates Src-dependent hypoxia-induced expression of VEGF in pancreatic and prostate carcinomas. *Oncogene*. 2005;24(19):3110–3120.
18. Gray MJ, Wey JS, Belcheva A, et al. Neuropilin-1 suppresses tumorigenic properties in a human pancreatic adenocarcinoma cell line lacking neuropilin-1 coreceptors. *Cancer Res.* 2005;65(9):3664–3670.
19. Landen CN Jr, Chavez-Reyes A, Bucana C, et al. Therapeutic EphA2 gene targeting in vivo using neutral liposomal small interfering RNA delivery. *Cancer Res.* 2005;65(15):6910–6918.
20. Arumugam T, Ramachandran V, Logsdon CD. Effect of cromolyn on S100P interactions with RAGE and pancreatic cancer growth and invasion in mouse models. *J Natl Cancer Inst*. 2006;98(24): 1806–1818.
21. Parikh AA, Fan F, Liu WB, et al. Neuropilin-1 in human colon cancer: expression, regulation, and role in induction of angiogenesis. *Am J Pathol*. 2004;164(6):2139–2151.
22. Camp ER, Yang A, Liu W, et al. Roles of nitric oxide synthase inhibition and vascular endothelial growth factor receptor-2 inhibition on vascular morphology and function in an in vivo model of pancreatic cancer. *Clin Cancer Res.* 2006;12(8):2628–2633.
23. Yang AD, Fan F, Camp ER, et al. Chronic oxaliplatin resistance induces epithelial-to-mesenchymal transition in colorectal cancer cell lines. *Clin Cancer Res.* 2006;12(14 pt 1):4147–4153.
24. Favier B, Alam A, Barron P, et al. Neuropilin-2 interacts with VEGFR-2 and VEGFR-3 and promotes human endothelial cell survival and migration. *Blood*. 2006;108(4):1243–1250.
25. Gluzman-Poltorak Z, Cohen T, Shibuya M, Neufeld G. Vascular endothelial growth factor receptor-1 and neuropilin-2 form complexes. *J Biol Chem.* 2001;276(22):18688–18694.
26. Fan F, Wey JS, McCarty MF, et al. Expression and function of vascular endothelial growth factor receptor-1 on human colorectal cancer cells. *Oncogene*. 2005;24(16):2647–2653.
27. Barleon B, Sozzani S, Zhou D, Weich HA, Mantovani A, Marme D. Migration of human monocytes in response to vascular endothelial growth factor (VEGF) is mediated via the VEGF receptor flt-1. *Blood*. 1996; 87(8):3336–3343.
28. Wey JS, Fan F, Gray MJ, et al. Vascular endothelial growth factor receptor-1 promotes migration and invasion in pancreatic carcinoma cell lines. *Cancer*. 2005;104(2):427–438.
29. Lesslie DP, Summy JM, Parikh NU, et al. Vascular endothelial growth factor receptor-1 mediates migration of human colorectal carcinoma cells by activation of Src family kinases. *Br J Cancer*. 2006;94(11): 1710–1717.
30. Jin KL, Mao XO, Greenberg DA. Vascular endothelial growth factor: direct neuroprotective effect in in vitro ischemia. *Proc Natl Acad Sci USA*. 2000;97(18):10242–10247.
31. Neufeld G, Cohen T, Gengrinovitch S, Poltorak Z. Vascular endothelial growth factor (VEGF) and its receptors. *FASEB J*. 1999;13(1):9–22.
32. Gerber HP, Dixit V, Ferrara N. Vascular endothelial growth factor induces expression of the antiapoptotic proteins Bcl-2 and A1 in vascular endothelial cells. *J Biol Chem.* 1998;273(21):13313–13316.
33. Gerber HP, McMurtrey A, Kowalski J, et al. Vascular endothelial growth factor regulates endothelial cell survival through the phosphatidylinositol 3′-kinase/Akt signal transduction pathway. Requirement for Flk-1/KDR activation. *J Biol Chem.* 1998;273(46):30336–30343.
34. Cai J, Ahmad S, Jiang WG, et al. Activation of vascular endothelial growth factor receptor-1 sustains angiogenesis and Bcl-2 expression via the phosphatidylinositol 3-kinase pathway in endothelial cells. *Diabetes*. 2003;52(12): 2959–2968.
35. Blume-Jensen P, Janknecht R, Hunter T. The kit receptor promotes cell survival via activation of PI 3-kinase and subsequent Akt-mediated phosphorylation of Bad on Ser136. *Curr Biol.* 1998;8(13):779–782.
36. Stoica BA, Movsesyan VA, Lea PMt, Faden AI. Ceramide-induced neuronal apoptosis is associated with dephosphorylation of Akt, BAD, FKHR. GSK-3beta, and induction of the mitochondrial-dependent intrinsic caspase pathway. *Mol Cell Neurosci*. 2003;22(3):365–382.
37. Yuan L, Moyon D, Pardanaud L, et al. Abnormal lymphatic vessel development in neuropilin 2 mutant mice. *Development*. 2002;129(20): 4797–4806.

Funding

National Institute of Health-5 T32 CA09599 (to G. V. Buren, N. A. Dallas, A. D. Yang, and S. Lim); Program Project Development Grant from the Ovarian Cancer Research Fund, Inc. (to A. K. Sood); the Zarrow Foundation (to A. K. Sood); The John E. and Dorothy Harris Fund for Gastrointestinal Cancer Research (to L. M. Ellis); The William C. Liedtke, Jr, Fund for Cancer Research (to L. M. Ellis); National Institutes of Health (RO1 CA112390 to L. M. Ellis).

Notes

The sponsors had no role in the study design, data collection and analysis, interpretation of the results, the preparation of the manuscript, or the decision to submit the manuscript for publication.

We thank Rita Hernandez (Department of Surgical Oncology) and Christine Wogan (Department of Scientific Publications) for manuscript editing and preparation.

Manuscript received May 15, 2007; revised October 25, 2007; accepted November 21, 2007.